Subproject B3.5

Nanoscale Quantum Memory for Superconducting Qubits

Principle Investigator: Alexey Ustinov

CFN-Financed Scientists: **Tobias Wirth (0.75 E13, 12 months),**
Pavel Bushev (1 E13, 1.5 months),
Ming He (0.5 E13, 1.5 months),
Hannes Rotzinger (1 E13, 1.5 months)

Further Scientists: **Jürgen Lisenfeld, Jared Cole, Clemens Müller, Alexander Shnirman, Alexander Lukashenko**

Physikalisches Institut
Karlsruher Institut für Technologie

Nanoscale Quantum Memory for Superconducting Qubits

Introduction and Summary

The subproject B3.5 is directed towards the investigation of quantum-coherent properties of atomic-scale dipole states in an amorphous dielectric forming tunnel barrier of a Josephson junction. These microscopic defects behave as quantum two-level systems (TLSs) and interact with the electrical field in the tunnel barrier of the junction. By using quantum mechanical manipulation of a superconducting qubit containing the Josephson junction we can directly access and manipulate individual TLSs and use them as a memory for the quantum state or even as independent qubits.

A superconducting phase qubit is a superconducting loop interrupted by a Josephson junction (JJ). The complexity of the superconducting circuits with phase qubits has been rapidly growing. Most impressive recent experiments were implemented with first multi-qubit circuits with several phase qubits entangled with each other [1]. Nonetheless, the main problem of these "artificial atoms" remains their relatively short coherence times. Although the energy relaxation time T_1 of the best phase qubits now approaches 1 μs, it persists being the limiting factor for the complexity of attainable quantum operations. The main source of decoherence is the unavoidable coupling of the qubit to a continuum of weakly coupled, short-living two-level systems (TLSs), which are mostly located in the tunneling barrier of the qubit junction. On the other hand, some TLSs are strongly interacting with the qubit and possess much longer coherence times. These TLSs can be used as independent two-level quantum systems for implementing, for example, quantum memory or computation tasks. Physical properties of individual TLS are until now poorly studied and their investigation could shed light on the microscopic nature of these defect states.

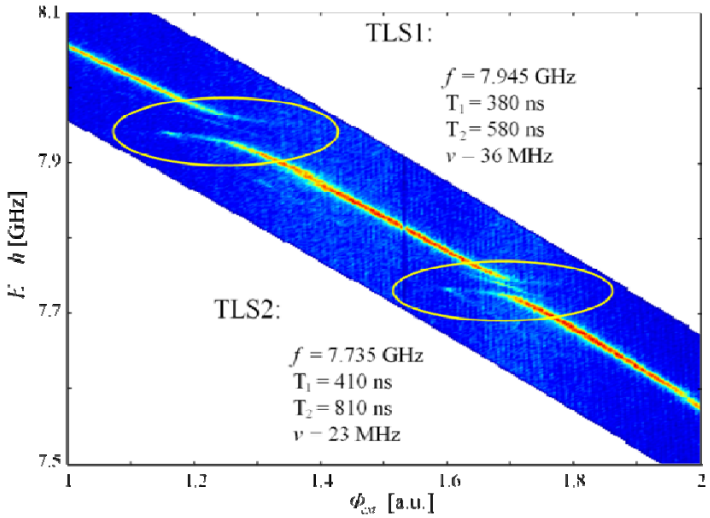

Figure 1: The spectrum of a qubit: The population probability of the excited qubit state is coded in color as a function of drive frequency and bias flux. The two level anti crossings reveal two TLSs that are strongly coupled to the qubit. Parameters f and v denote the TLS resonance frequency and the coupling, respectively. The relaxation time T_1 and the dephasing time T_2 of both TLSs are significantly longer than those of the qubit (~100 ns). We denote the upper (lower) TLS as TLS1 (TLS2).

Most of our experiments were made with qubit circuits fabricated in the group of J. M. Martinis (UCSB) [2]. Overall, this subproject was very successful and productive. We have published 4 papers: two in Physical Review [B3.5:1,B3.5:2] (one of them as Rapid Communication), one in

Applied Physics Letters [B3.5:3], and one in Physical Review Letters [B3.5:4]. Besides that, one very important paper on entanglement between two TLSs coupled via qubit is now prepared for publication [B3.5:5].

After the cool-down we found the qubit strongly coupled to two TLSs which showed up to four times longer coherence times than those of the qubit. The qubit spectrum with signatures of these two TLSs is presented in Fig.1. We experimentally investigated the coupling mechanism between the qubit, TLS and microwaves, which lead to a very detailed and complete theoretical picture [B3.5:1,B3.5:2]. By comparing our experimental data with current models proposed for the microscopic origin of TLSs, we verified the applicability of several alternative models for coupling between qubit and TLSs [B3.5:3]. We also characterized the coherence times of two specific TLSs in dependence on temperature [B3.5:4]. Finally, we showed the ability to coherently manipulate the TLSs by the qubit and implemented entanglement of two TLSs [B3.5:5].

1. Investigation of the coupling mechanism between qubit and TLS

1.1 Coupling of a TLS to the microwave field [B3.5:1]

When the microwave drive is tuned in resonance with the qubit, i.e. when the energy of the photons is equal to the energy separation between the ground and the excited state of the qubit, one expects observing Rabi oscillations. In this case the probability of the occupation of the excited state oscillates as a function of time, and the frequency of these probability oscillations depends on the microwave driving power and detuning from the resonance.

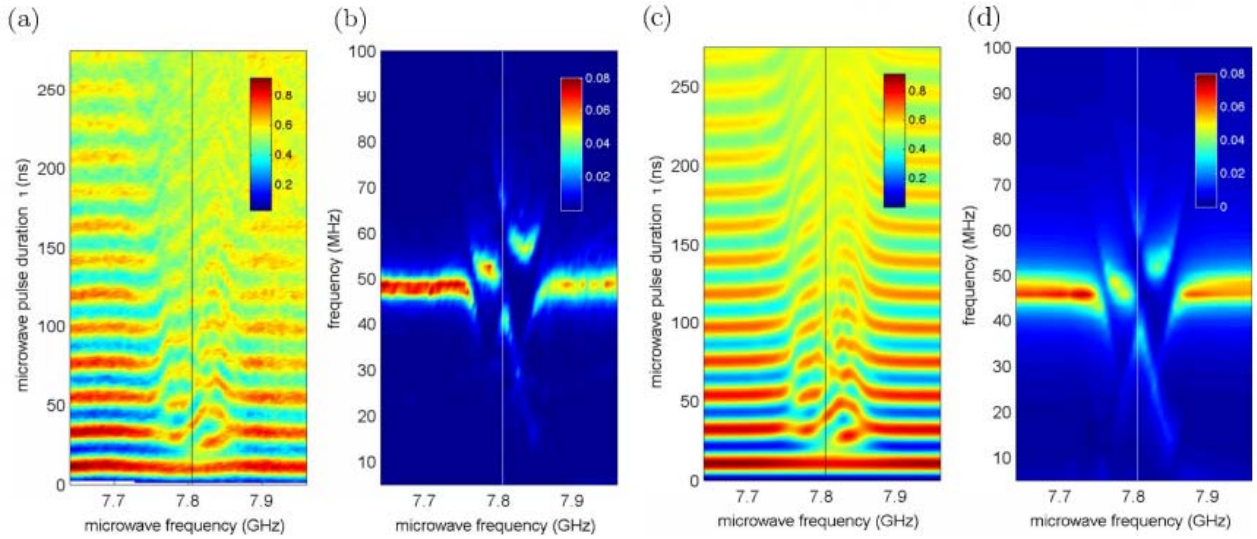

Fig. 2: Experimentally observed (a) and simulated (c) time evolution of the probability to measure the qubit in the excited state when it is resonantly driven, in dependence on the qubit frequency which expands over the TLS frequency [B3.5:1]. (b) and (d) show the corresponding Fourier transformations.

The experiment performed by J. Lisenfeld et al. [B3.5:1] was to observe Rabi oscillations of the qubit strongly coupled to a TLS. When the qubit was biased near the resonance with the TLS, the dynamics become quite complicated. The measured probability of the qubit occupation of the excited state depending on the time and frequency is presented in Fig. 2(a). Its Fourier transformation is shown in Fig. 2(b). The asymmetry between the microwave frequencies below

and above the resonance with the TLS at about 7.8 GHz can be clearly seen. This asymmetry cannot be reproduced theoretically without assuming an additional coupling between the TLS and microwaves. To get the calculated pictures Fig. 2(c),(d) one has to take such coupling between the TLS and microwaves into account. The explanation for this behavior is based on an effective coupling due to virtually induced transitions through the second excited state of the qubit. When the qubit is in its first excited state $|1\rangle$, a second order Raman-type process can occur, where the next higher level of the qubit $|2\rangle$ is virtually excited followed by an excitation of the TLS and a transition of the qubit to the state $|1\rangle$. Since this process depends on the energy difference between the states $|1\rangle$ and $|2\rangle$, the important parameters for the coupling strength between TLS and microwave are the detuning between the qubit and TLS and the anharmonicity of the qubit potential.

1.2 Multi-photon spectroscopy [B3.5:2]

The second experiment that we performed with the same system demonstrates the excitation of the coupled TLS-qubit hybrid quantum system by single and/or double photon absorption [B3.5:2]. Figure 3 shows the usual level anti-crossing measured by microwave spectroscopy at low power. The upper branch corresponds to the $|1+\rangle$ state and the lower one to the state $|1\text{-}\rangle$, where these states are defined as $|1\pm\rangle=|0e\rangle\pm|1g\rangle$ and $|g\rangle$ and $|e\rangle$ denote the ground and excited state of the TLS. The middle line between these two states occurs due to the two-photon transition from the ground state to the double excited state $|1e\rangle$, the required energy is $E_{1e}/2 = E_{1g}/2 + E_{0e}/2$. Thus, when slightly changing the qubit frequency, the line corresponding to the $|1e\rangle$ state is expected to have a slope of 1/2 relative to the slope of the main transition between qubit states $|0\rangle$ and $|1\rangle$.

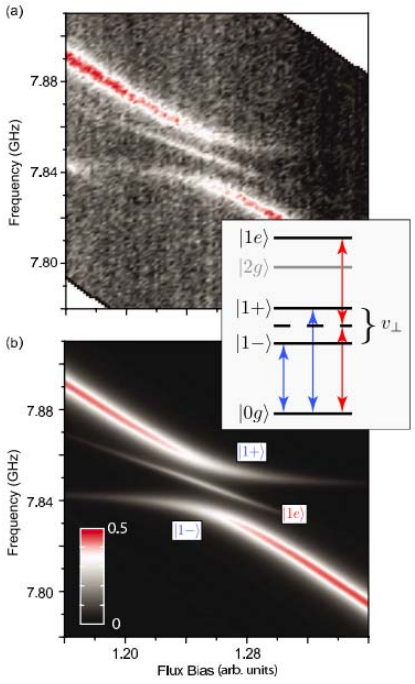

Figure 3: Spectroscopy of single photon transition at low power. (a) Experiment, (b) Simulation

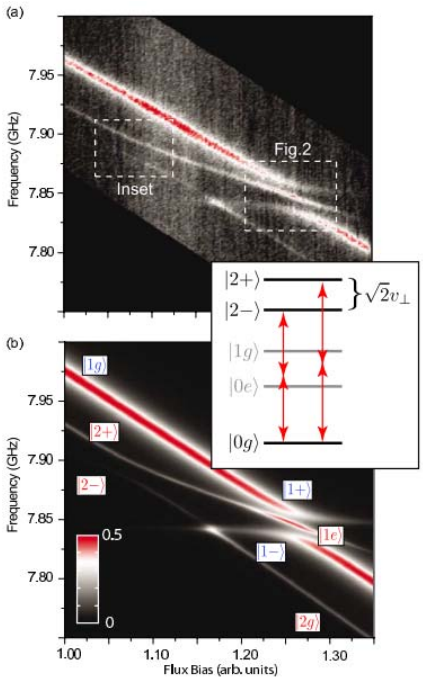

Figure 4: Spectroscopy of single and two-photon transition at high power. (a) Experiment, (b) Simulation

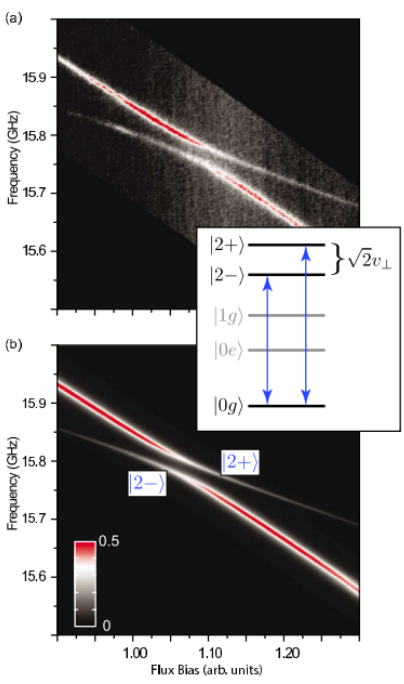

Figure 5: Spectroscopy of single photon transition at double frequency. (a) Experiment, (b) Simulation

If the microwave power is increased, more lines become visible in the spectrum. The thin line in Fig. 4 below the main resonance of the qubit is the double photon absorption that brings the qubit to the second excited state. Due to the anharmonicity of the potential, the energy difference between the states $|2g\rangle$ and $|1g\rangle$ is smaller than between $|1g\rangle$ and $|0g\rangle$, so that it will cross the $|1e\rangle$ line. Here, another avoided level crossing can be observed, yielding the new hybridized states $|2\pm\rangle=|1e\rangle\pm|2g\rangle$. Another interesting point is the crossing of the lines corresponding to $|2g\rangle$ and $|0e\rangle$. This is a point of high absorption, since the energies $E_{2g}$and E_{2e} are multiples of the TLS's energy, so that even the $|2e\rangle$ state gets populated. Once the microwave frequency is doubled, as shows Fig. 5, only single photon absorption becomes possible, showing the transition to the states $|2g\rangle$ and $|1e\rangle$ and their hybridization $|2\pm\rangle$.

1.3 Identifying the coupling mechanism between qubit and TLSs [B3.5:3]

The full expression of the Hamiltonian of the qubit reads

$$H_q = \frac{2e^2}{C}\hat{q}^2 - E_J \cos\hat{\varphi} + \frac{1}{2L}\left(\frac{\Phi_0}{2\pi}\right)^2 (\hat{\varphi} - \varphi_{Ext})^2,$$

where the first term describes the charge energy of the JJ, the second term is the potential of the JJ with the Josephson energy E_J and the third term is responsible for the magnetic energy generated in the superconducting loop. As one can see, there are three different possibilities for TLSs to couple to the qubit: by the charge operator $\hat{q}$, by the phase operator $\hat{\varphi}$ or by the operator $\cos\hat{\varphi}$. In the first case the TLS couples to the electric field in the JJ. This corresponds to the usual explanation of TLSs which are said to be charge dipoles and in this case there is no longitudinal coupling. The second mechanism is associated with a variation of the critical current of the JJ (E_J depends on I_C), which allows also longitudinal coupling. An example is an impurity in the JJ which hybridizes with the Cooper pairs tunneling through the junction. The last mechanism describes coupling to the external flux threading the superconducting loop, which is reasonable if a TLS is assumed to be a spin on the surface of the superconductor. Here, also longitudinal coupling is possible, since the state of the spin has an effect on the magnetic energy of the qubit.

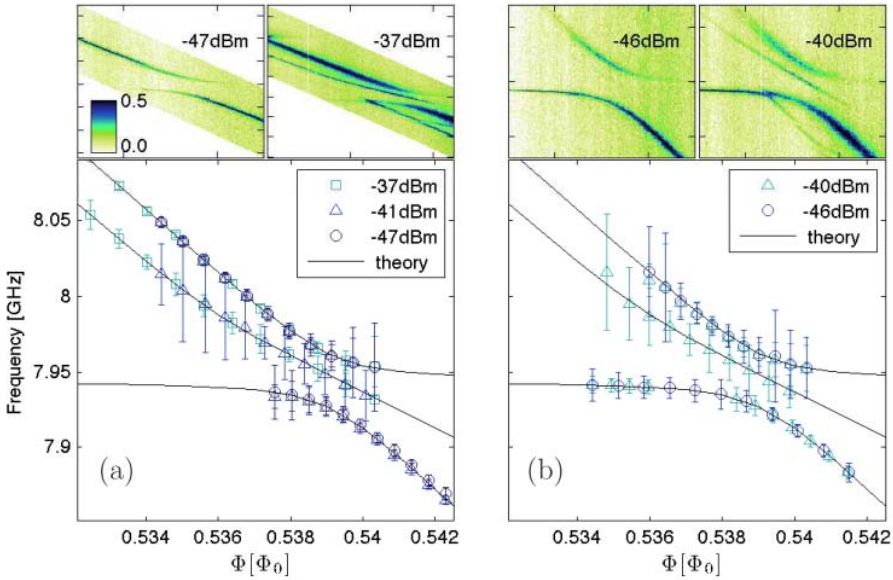

Figure 6: Peak positions obtained for (a) qubit spectroscopy and (b) swap spectroscopy. The theoretical curves show the relevant transition frequencies for the coupled qubit-TLS system obtained via fitting the extracted peak positions.

TLS1	ϵ_{TLS}	$v_\perp$	$v_\parallel$	χ_r^2
$H_I^{(p)}$	7944.49 ± 0.08	35.65 ± 0.08	$----$	0.998
$H_I^{(\phi)}$	7944.41 ± 0.08	35.55 ± 0.09	0.23 ± 0.12	0.997
$H_I^{(c)}$	7944.38 ± 0.08	35.52 ± 0.13	0.27 ± 0.12	0.997
TLS2	ϵ_{TLS}	$v_\perp$	$v_\parallel$	χ_r^2
$H_I^{(p)}$	7734.0 ± 0.2	23.2 ± 0.2	$----$	0.994
$H_I^{(\phi)}$	7734.5 ± 0.2	23.3 ± 0.2	0.5 ± 0.2	0.992
$H_I^{(c)}$	7734.4 ± 0.3	23.3 ± 0.2	0.5 ± 0.2	0.992

Table 1: TLS resonance frequency and qubit-TLS coupling which were obtained from the fitting procedure. The strength of the longitudinal coupling is lying in the uncertainty range. The reduced χ^2 value is also given for each fit showing good convergence.

By comparing the predictions of different models with experimental data we expected to be able to favor or rule out some of TLS-qubit coupling theories . Therefore we performed high precision ($f \sim$ 8 GHz, 1-σ interval ~ 15 MHz) single and double photon spectroscopy and swap spectroscopy of TLS1 and TLS2, see Fig. 6. Swap spectroscopy here means swapping of the TLS state on the qubit before the readout. We estimated the coupling parameters and the goodness of the fit for these general theories (Tab.1). As one can see, all models yielded reasonable values so that in principle all three coupling mechanisms are feasible. The longitudinal coupling component $v_\parallel$, if present, is very small in comparison to the dominating transverse coupling $v_\perp$. Since it is even lying in the uncertainty range, it is a good approximation to neglect it completely in most cases.

2. Temperature dependence of TLS coherence times [B3.5:4]

An important experiment that can shed light on the physical nature of intrinsic TLSs is measurement of the temperature dependence of the TLS coherence. The excitation of the TLS is performed by using our newly developed method of direct TLS control by the microwave field, see Fig. 7. The readout is managed via swapping the state of the TLS with the qubit. By exciting the TLS with a π-pulse and measuring its exponential decay, the relaxation time T_1 can be extracted. The Ramsey experiment yields the characteristic time T_2. Here, two π/2-pulses are applied on the TLS with different time intervals in-between. The characteristic times T_1, decay of Rabi oscillations and T_2 versus the detuning of the qubit relative to the TLS frequency are shown on the plots Fig. 7(d)-(f). The results are $T_1^{TLS1} \approx 380$ ns, $T_2^{TLS1} \approx 580$ ns, $T_\varphi^{TLS1} \approx 2.45$ µs, and $T_1^{TLS2} \approx 410$ ns, $T_2^{TLS2} \approx 810$ ns, $T_\varphi^{TLS2} \approx 66$ µs, where the pure dephasing time T_φ is calculated via the equation $T_\varphi^{-1} = T_2^{-1} - (2T_1)^{-1}$. In the case of TLS2, $T_2^{TLS2} \approx 2T_1^{TLS2}$, i.e. no excess dephasing was found giving rise to the large pure dephasing time. For TLS1, this is not the case, however, the Hahn echo experiment (an additional π-pulse between two π/2-pulses, see Fig. 8) enhances the dephasing time T_2^* to 743 ns which corresponds to $2T_1^{TLS1}$. It can be thus concluded that the dephasing mechanism in TLS1 is dominated by low frequency energy fluctuations. Finally, we measured for the first time all these times as a function of temperature, see Fig. 9. The decrease of the characteristic times could be fitted with a quadratic function. We did not observe any variation of the TLS' resonance frequency and coupling strength to the qubit with temperature.

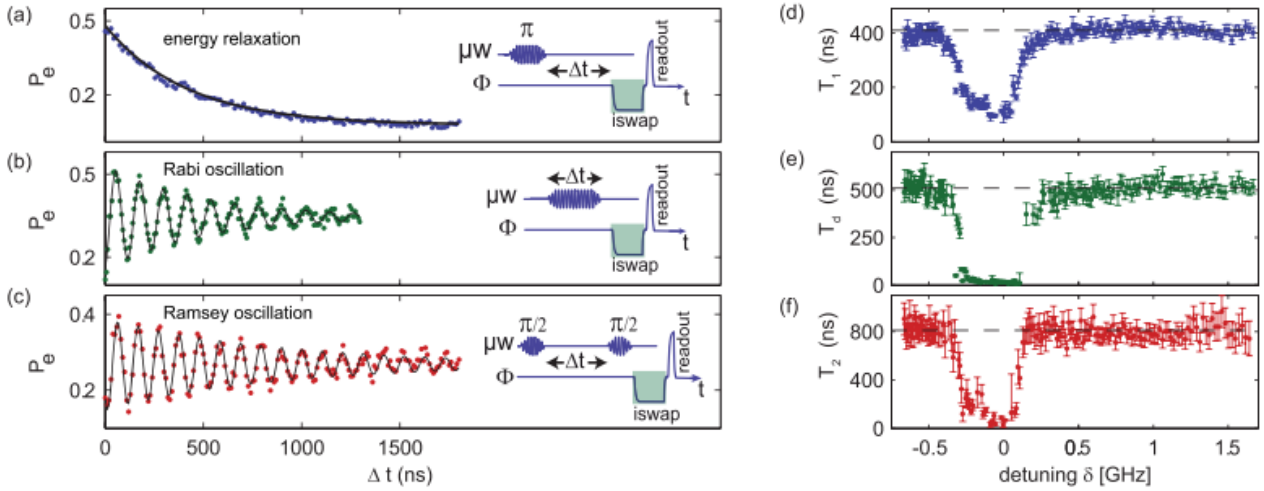

Fig. 7: Coherent response of TLS2 to standard microwave pulse sequences as depicted in the insets: (a) Relaxation. (b) Decay time of Rabi oscillations. (c) Decay time of Ramsey oscillations (microwave detuned from TLS by 10 MHz). Panels (d), (e) and (f) show the energy relaxation time T_1, the Rabi decay time T_d, and the dephasing time T_2 of TLS1 in dependence on the detuning δ between TLS1 and qubit.

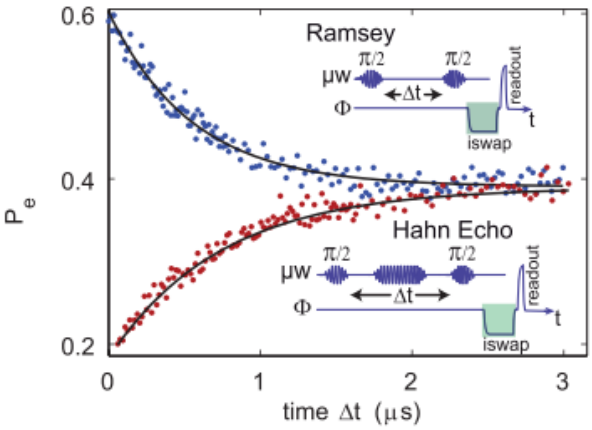

Fig. 8: Echo amplitudes obtained from Ramsey (blue) and Hahn echo (red) sequences for TLS1. Estimated dephasing times: 551 ± 41 ns (Ramsey) and 743 ± 62 ns (Hahn echo).

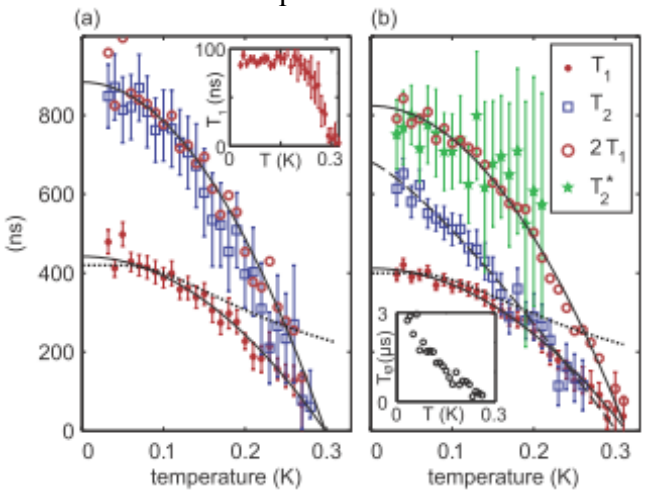

Fig. 9: Temperature dependence of coherence times in (a) TLS 1 and (b) TLS 2. Solid lines are parabolas. Inset: (a) Temperature dependence of the qubit T_1 time. (b) Extracting pure dephasing time T_φ.

3. Coherent manipulation and entanglement of two TLS [B3.5:5]

In this experiment, we established a coherent interaction between TLS1 and TLS2 via the qubit, yielding entanglement between the two TLSs. The pulse sequence is shown in Fig. 10. After the excitation of the qubit with a π-pulse, it performs a $\sqrt{\text{iSWAP}}$ with TLS2 resulting in entanglement between the qubit and TLS2. Then, the qubit is tuned to different frequencies ω_h and is kept there for the holding time t_h. Before the qubit is read-out, it performs a second $\sqrt{\text{iSWAP}}$ with TLS2. The two $\sqrt{\text{iSWAP}}$s lead to an interference pattern, since, depending on the holding position and time of the qubit between the two operations, the qubit accumulates a different phase in comparison to TLS2 so that a constructive or destructive interference can be observed in Fig. 11(a),(c). The slowest oscillations are at resonance with TLS2, which corresponds to energy oscillations between

the qubit and TLS2. Around this resonance the frequency increases, imitating a chevron pattern. The interesting part is, however, at frequencies ω_h around the resonance of TLS1. Here, an additional chevron pattern can be observed. The oscillations at resonance with TLS2 and with TLS1 are plotted in Fig. 12(a) and (b), respectively.

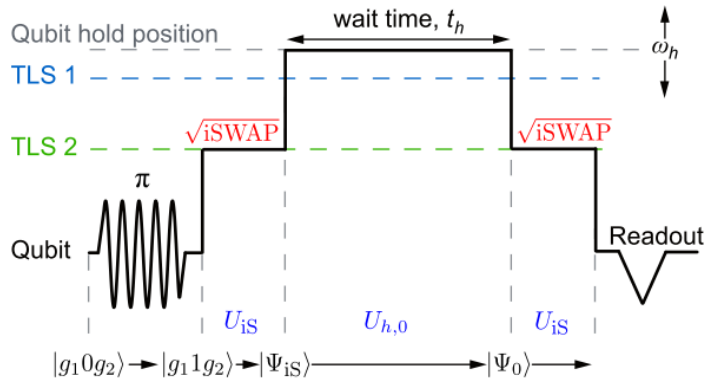

Fig. 10: The experimental TLS manipulation and measurement sequence [B3.5:5].

We performed a simulation of the complete system consisting of three two-level quantum systems and obtained a very good agreement with the experiment. The vanishing and the reappearing of the oscillations at the resonance with TLS1 can be explained by oscillations of the population of the qubit with TLS1. Note, that even after the excitation of the qubit has swapped to TLS1 and back to the qubit, the qubit still shows constructive and destructive interference with TLS2. From this we can conclude that at the times when TLS1 is excited, it is entangled with TLS2.

Figure 11(a) shows this situation before the second $\sqrt{\text{iSWAP}}$. As expected, half of excitation is in TLS2 and decays exponentially (when neglecting the small oscillations due to coupling to the qubit) and the other half oscillates between the qubit and TLS1. In Fig. 13(b) the concurrence between each two subsystems (measurement of the entanglement) is plotted versus holding time. It can be seen that the entanglement is oscillating between qubit-TLS2 and TLS1-TLS2, and the entanglement between qubit and TLS1 oscillates with double frequency (maximal entanglement between qubit and TLS1 occur twice a cycle) and has only half amplitude.

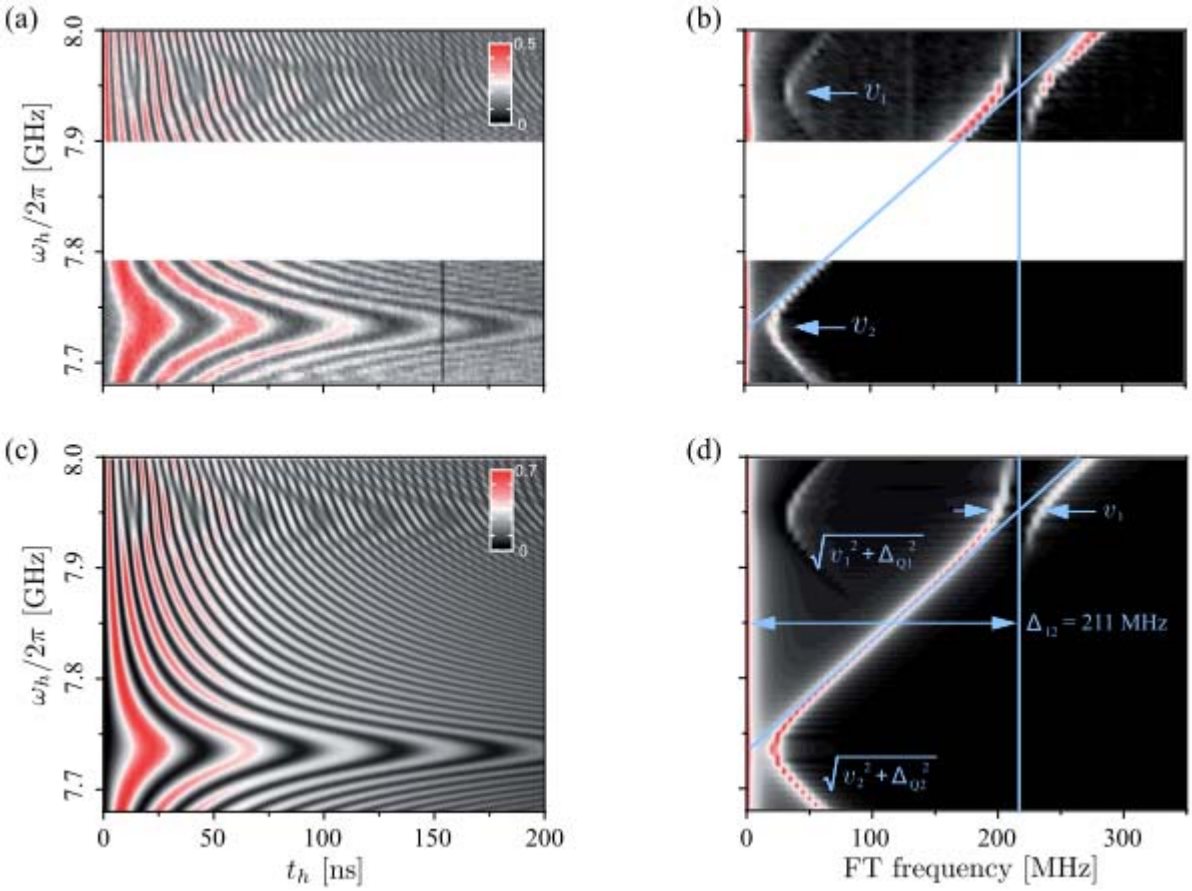

Fig. 11: Experimental (a) and theoretical (c) beating signal of the qubit state with two TLSs. Experimental (b) and theoretical (d) Fourier transform of the beating signal. The anti-crossing on TLS2 hyperbola indicates the established interaction between two defects via the phase qubit [B3.5:5].

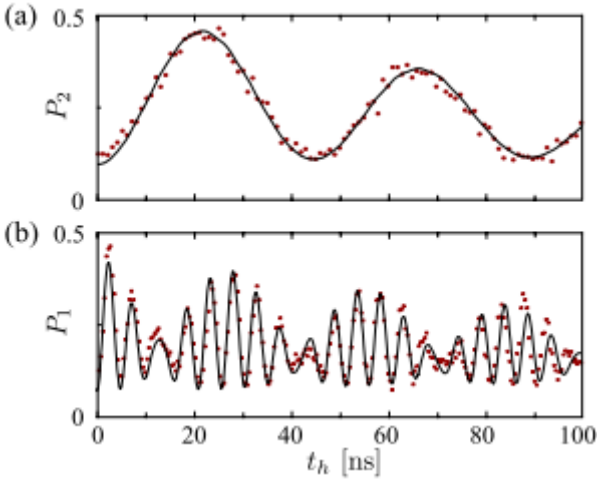

Fig. 12: The simulation (solid) and measurement (dots) at the holding position of the qubit in resonance with TLS2 (a) and TLS1 (b) [B3.5:5].

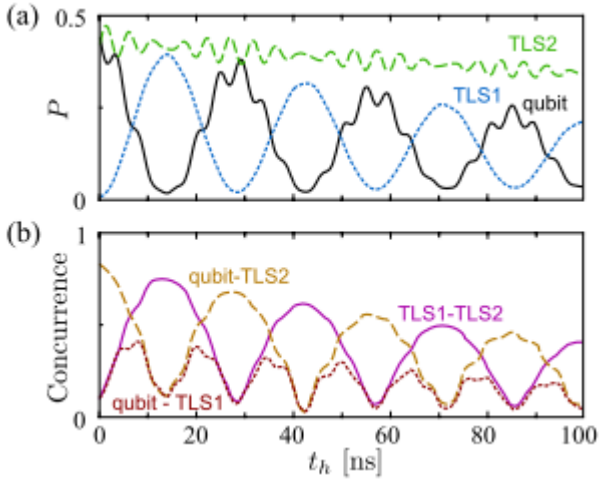

Fig. 13: (a) Simulated excitation probabilities of the three subsystems while holding the qubit at resonance with TLS1 for the time t_h. (b) Simulated concurrence between each individual pair of subsystems [B3.5:5].

4. Service for other CFN Projects

The experimental work performed within B3.5 was done in close interaction with the CFN theoretical group of led by Alexander Shnirman and Gerd Schön within the subproject B3.3. This interaction led to our joint publications [B3.5:1- B3.5:5]. Besides that, better understanding of the physical properties of individual TLSs achieved in this subproject is vitally important also for subproject B1.5 dealing with characterization of decoherence in dielectrics used for fabrication of superconducting quantum circuits. In subproject B1.5 we have been closely collaborating with Michael Siegel and Georg Weiß.

References

- own work with complete titles -

[1] M. Neeley, R. C. Bialczak, M. Lenander, E. Lucero, M. Mariantoni, A. D. O'Connell, D. Sank, H. Wang, M. Weides, J. Wenner, Y. Yin, T. Yamamoto, A. N. Cleland, and J. M. Martinis, Nature **467**, 570 (2010)
[2] M. Steffen, M. Ansmann, R. McDermott, N. Katz, R. C. Bialczak, E. Lucero, M. Neeley, E. M. Weig, A. N. Cleland, and J. M. Martinis, Phys. Rev. Lett. **97**, 050502 (2006)